Progress in Additive Manufacturing
https://doi.org/10.1007/s40964-022-00296-5

FULL RESEARCH ARTICLE

Improving the fatigue life of printed structures using stochastic variations

Sander van den Broek[1] · Johannes Wolff[2] · Sven Scheffler[1] · Christian Hühne[2] · Raimund Rolfes[1]

Received: 10 July 2021 / Accepted: 27 March 2022

Abstract
Additive manufacturing allows designers to create geometries that would not be possible or economical to manufacture using traditional manufacturing processes. Production with these technologies does, however, introduce a large amount of variation and additional unknowns. These random variations from idealized geometry or material properties can harm the performance of the design. The current work presents an approach to improve the fatigue life of such structures, and simultaneously reduce its influence from random variations in local thickness. Following an initial numerical study, the results are experimentally validated. Experimental results show a significant improvement in fatigue life in the redesigned sample with a tailored thickness distribution.

Keywords Random field · Robust design · Fatigue improvement · Thickness tailoring · Additive manufacturing

1 Introduction

Load conditions of structures often change during operation. Cyclic changes in the stress state of a structure can cause cumulative damage, leading to fatigue failure after a certain number of cycles. Certain structural features, such as holes, slots, and sharp edges, cause stress concentrations that accelerate fatigue failure. For many of these features, it is best to avoid them, but holes are sometimes necessary due to cable routing, water drainage, pressure-equalizing, or other reasons. Designs can be adapted in these cases to minimize any adverse effects and reduce the effects of stress concentrations, which can induce fatigue failure.

Additive Manufacturing (AM) is a term used for different manufacturing technologies that create a structure by successively adding material layer by layer [15, 16]. A wide range of materials can be used with these techniques, including metals, polymers, and resins. These techniques selectively place or harden material using direct printing, laser sintering, photopolymerization, or another process.

✉ Sander van den Broek
s.vandenbroek@isd.uni-hannover.de

[1] Institute of Structural Analysis, Leibniz University Hannover, Appelstr. 9A, 30167 Hannover, Germany

[2] Deutsches Zentrum für Luft-und Raumfahrt (DLR), Lilienthalplatz 7, 38108 Brunswick, Germany

The extra design freedom offered by AM techniques allows for an economical fabrication of components with very complex geometries, which are not feasible with traditional manufacturing techniques [28]. Nevertheless, since different AM techniques exhibit different design limitations, it is crucial to keep process type and necessary support structures in mind during planning and designing. Manufacturability can be assured by adding constraints to the topology optimization by adding length-scale controls [25, 39], non-enclosed void [27], and overhang constraints that limits the geometry to shapes which are less likely to collapse during manufacturing [23, 31]. Some AM technologies also cause an anisotropic behavior of the printed components, which must be taken into account during the design process [7].

The fatigue behavior can be improved using a design process that shapes the structure to minimize stresses within a given design volume [30]. Keshavarzzadeh et al. [20] showed that a more robust design with respect to random variations of geometry, material, and loads is possible by taking random variations into account during the design process. When it comes to fatigue, there are some hurdles to overcome in specific AM processes.

The most popular process used for polymers is Fused Filament Fabrication (FFF). FFF involves extruding molten plastic filament through a movable nozzle. Strands between 0.05 and 0.8 mm in diameter are deposited parallel in two-dimensional layers and fused to the previous layer during

Published online: 18 April 2022

deposition. In this way, a layer-by-layer manufacturing process generates three-dimensional components. Within the FFF process, Chacón et al. and Wu et al. [5, 38] showed that the stiffness, strength, and fatigue performance of a printed component are directly influenced by manufacturing process parameters such as the printing direction as well as the equipment used. Generally, the build-up direction is less robust and more susceptible to brittle failure than other directions [5]. Another parameter is the raster angle, referring to the printing direction which dominates in a layer. The ideal raster angle depends on the load and resulting stresses in the structure, the desired stiffness [26, 38], and fatigue requirements [13]. The extrusion and nozzle movement also influences the thickness of printed layers. The exact effects of the change in layer thickness vary depending on the build-up direction and stress state of the structure.

In most cases, it is advantageous to orient the raster angle in the main direction of the load, thereby orienting the filaments into the principal stress. Other design and process parameters can also influence the material parameters, such as the type of reinforcement used in fiber-reinforced filaments and the fiber volume fraction [6]. Predicting the exact mechanical properties of the manufactured materials becomes quite complex, especially when variations introduced by machine and filament batch are also taken into account. Work done by Zou et al. [40] tries to predict mechanical properties while varying some of the discussed parameters, but these are still only estimates given to the inherent complexity.

These parameters can affect the semi-crystalline structure of an FFF structure, but more importantly, affect the bonding of filaments added at every layer. With the right printing parameters, Young's modulus within a printed layer can be nearly identical in longitudinal and transverse directions. In the buildup direction the Young's modulus can vary due to inter-layer contact differences and polymer crystallization. Conversely, the ultimate tensile stress in the buildup direction is usually significantly lower, showing more brittle behavior than in the printing plane [33]. Analysis of experimental results by Ezeh and Susmel [13] shows that the logarithmic slope in an s-n curve is the same in all directions when scaled from the ultimate tensile stress.

Even when the best effort is made to control manufacturing parameters, an increase relative to traditional approaches still exists in the uncertainty in the material's strength, stiffness, and fatigue resilience. Controlling the process and assuring consistent performance is much more complex with an additive manufacturing technique such as FFF than traditional approaches, e.g., injection molding. Many opportunities exist in the FFF process for improper adhesion to form between filaments and for voids to form between filaments and layers in a structure, to name two sources of imperfections. Work done by Iragi et al. [19] has shown that a large amount of deviation from the expected performance can be traced down to such microstructure imperfections that are introduced during manufacturing.

Overcoming these uncertainties introduced by FFF manufacturing to improve fatigue life requires a robust design that is not as quickly affected by variations. This paper presents an approach for improving the fatigue life of a thin-walled, FFF-manufactured structure by a mass-neutral shape adaptation. Herein, only the thickness is varied, which is of particular interest for thin-walled structures in which the shape is fixed due to e.g., aerodynamic flow considerations. An example of this would be the inner structure of a suction-panel wing-box designed to facilitate laminar flow over the outer surface of an aircraft wing. Such a structure may consist of gyroid unit cells of varying sizes to facilitate a specific pressure drop. Herein, the thickness of the unit cells can be varied to reduce stress-induced fatigue while not having a significant effect on the internal airflow. The approach used in this paper utilizes stochastic analyses to simulate the effects of local changes in thickness. Then, through post-processing, the correlation is computed between local thickness changes and the estimated influence on the fatigue life. Such a correlation pattern gives a map of the influence local changes have on fatigue life. Applying this pattern to modify the local thickness of the structure tailors the structure to increase its fatigue life. Using an open-hole structure as an example the approach is demonstrated numerically in Sect. 3, leading to a modified thickness distribution of the original design. Following numerical analyses, a series of experiments demonstrate the potential of this approach on an actual FFF open-hole specimen is presented in Sect. 4.

2 Methodology

The approach used to improve the fatigue life of a structure is based on earlier work on buckling loads presented in [3, 4]. This approach uses random fields to generate random patterns of thickness distributions within a thin-walled structure. These variations are compared to their effect on initial fatigue failure, generating a pattern of correlated values. Using this pattern material is redistributed, postponing initial failure, while at the same time creating a more robust structure.

2.1 Random field generation

Random thickness distributions are generated using random fields. Many techniques exist to generate random fields [18, 34]. Fields can be represented through continuous functions in space, usually a sum of functions. Sums of functions can be generated through a Karhunen-Loéve (KL) expansion [35] or Fourier series for instance [22]. Another approach is to

generate fields directly on points in space (such as nodes in a finite element model). Fields can be generated on those points through decomposition of the covariance matrix [8], using spatial averaging [36] or fast Fourier transformations [32].

Vectors representing values of the field on finite element nodes are generated using a technique known as Covariance Matrix Decomposition (CMD). CMD makes it possible to create random vectors in which entries have a specified correlation to each other. The choice for CMD is made because it is easy to implement, accurate, and has few limitations, especially for small to mid-sized models. The current approach generates fields using the finite element model nodes, giving thickness values at every structural node. Within the current work, correlation is a function of the physical distance between points on the structure. Correlation of two points i and j in field $\mathbf{h}$ is defined as [9, ch. 10]

$$\rho_{h_i,h_j} = \frac{\operatorname{cov}(h_i,h_j)}{\sigma_i\sigma_j} = \frac{\mathrm{E}\left[(h_i-\mu_i)(h_j-\mu_j)\right]}{\sigma_i\sigma_j}, \tag{1}$$

where E is the expectation operator and equals the mean value over an infinite amount of samples. Parameters μ and σ are the mean and standard deviation. The functions used within this work to determine the correlation of points on the structure to each other are

$$\rho_I = e^{-\frac{\Delta L}{L_c}} \tag{2}$$

and

$$\rho_{II} = e^{-\left(\frac{\Delta L}{L_c}\right)^2}, \tag{3}$$

where ΔL is the distance between points, and L_c is the correlation length. These two functions will, from now on, be referred to as type I and type II correlation functions. Both type I and II correlation functions are commonly used in literature, but generate fields that have different types of imperfections. Both types of fields are used in this work as a comparison, and in an analysis of imperfection sensitivity.

Generating a field requires first calculating the distances between nodes; these distances are then used to generate a correlation matrix using Eqs. (2) and (3). Assembly results in a symmetric positive definite correlation matrix with indices and matrix representation in the form of

$$R_{ij} = \frac{\operatorname{cov}(h_i,h_j)}{\sigma_i\sigma_j} \tag{4}$$

$$\mathbf{R} = \begin{bmatrix} 1 & \rho(h_1,h_2) & \dots & \rho(h_1,h_n) \\ \rho(h_2,h_1) & 1 & \dots & \rho(h_2,h_n) \\ \vdots & & \ddots & \vdots \\ \rho(h_n,h_1) & \rho(h_n,h_2) & \dots & 1 \end{bmatrix}. \tag{5}$$

CMD makes it possible to generate many fields without any additional computational cost. Most of the computing time is spent factorizing the correlation matrix, which has to be done only once. After precomputing, simple matrix multiplication can generate additional fields using a random zero-mean unit variance vector χ in the form

$$\mathbf{h} = \mathbf{L}\chi, \tag{6}$$

where $\mathbf{L}$ is a decomposed version of the correlation matrix $\mathbf{R}$ of Eq. (5).

Determining the decomposed correlation matrix is done by first taking the definition of covariance

$$\operatorname{cov}[h_i,h_j] = \mathrm{E}[h_ih_j] - \mathrm{E}[h_i]\mathrm{E}[h_j], \tag{7}$$

keeping in mind that the field has a zero mean value. The correlation matrix $\mathbf{R}$ can be decomposed into two matrices as

$$\begin{aligned} \mathbf{R} &= \operatorname{cov}[\mathbf{h},\mathbf{h}] = \mathrm{E}\left(\mathbf{h},\mathbf{h}^T\right) - 0\cdot 0 \\ &= \mathrm{E}\left[\mathbf{L}\chi(\mathbf{L}\chi)^T\right] = \mathbf{L}\mathrm{E}\left(\chi\chi^T\right)\mathbf{L}^T = \mathbf{L}\mathbf{I}\mathbf{L}^T = \mathbf{L}\mathbf{L}^T, \end{aligned} \tag{8}$$

where $\mathbf{I}$ is an identity matrix. This approach exploits the independence of the components of χ. Decomposition can be done using a variety of methods, such as Cholesky or eigenvalue methods. Within the current implementation, the eigenvalue decomposition was utilized, as this was shown to be slightly more accurate by van der Have [17]. Eigendecomposition gives matrices in the form

$$\mathbf{R} = \mathbf{Q}\boldsymbol{\Lambda}\mathbf{Q}, \tag{9}$$

where $\boldsymbol{\Lambda}$ is a diagonal matrix with eigenvalues of $\mathbf{R}$ on the diagonal, and $\mathbf{Q}$ contains its eigenvectors.

From this decomposed matrix the decomposed matrix $\mathbf{L}$ can be extracted as

$$\mathbf{R} = \mathbf{Q}\hat{\boldsymbol{\Lambda}}\hat{\boldsymbol{\Lambda}}\mathbf{Q} = \mathbf{L}\mathbf{L}^T \rightarrow \mathbf{L} = \mathbf{Q}\hat{\boldsymbol{\Lambda}}, \tag{10}$$

in which $\hat{\boldsymbol{\Lambda}} = \operatorname{diag}(\sqrt{\lambda})$, in which λ are the eigenvalues of the correlation matrix Eq. (5).

While solving the finite element model the thickness at integration points is evaluated at integration points using shape functions and field values at nodes. Fields are generated with unit variance and zero mean, the thickness at point i is therefore

$$t_i = t_\mu + h_i t_\sigma, \tag{11}$$

where h_i is the field value at point i and t_σ the standard deviation of thickness.

2.2 Improving the cycles until initial failure

Within the current approach, the number of cycles until initial failure is estimated using the highest stress within the structure. Structures printed using fused filament fabrication have a very similar Young's modulus in the printing plane, and slightly less stiff between printed layers. Elastic behavior for thin-walled structures can, therefore, be approximated as isotropic [5, 33, 40]. Experimental work done by Afrose et al., [1, 11, 12, 26] have indicated that the slope of the s-n diagram of the material is not dependent on the orientation of the printing direction. The structure designed has a primary filament orientation aligned with the applied forces. Inter-layer stresses should be minimal. With this in mind, it is possible to estimate the effect on the number of cycles using the Von Mises yield criterion and the material's SN curve. This allows the initial failure of the structure due to fatigue to be estimated from the stress state of the structure at a given thickness distribution.

Stress concentrations caused by the production process are not taken into account in this fatigue model, the estimated values are therefore a likely overestimation of the actual number of cycles until failure, and should therefore only be taken as a qualitative measure. Parameters affecting failure in tested specimens are further discussed in Sect. 4.4.1.

2.2.1 Calculating the correlation pattern

In a large set of random thickness patterns, some samples will show an increased number of cycles until failure, while others will show a decrease. A non-dimensional map of the average contribution of thickness to the critical stress state can be evaluated by computing the correlation of these at every point on the structure. If we create a pattern $\boldsymbol{H}$ of the thickness distribution and insert it into the mathematical definition of correlation (Eq. 1) we can compute its terms as

$$H_i = \frac{\sum_{j=1}^{n} \left(\sigma_{vm,j} - \bar{\sigma}_{vm}\right)\left(t_{i,j} - \bar{t}\right)}{\sqrt{\sum_{j=1}^{n} \left(\sigma_{vm,j} - \bar{\sigma}_{vm}\right)^2} \sqrt{\sum_{j=1}^{n} \left(t_{i,j} - \bar{t}\right)^2}}, \tag{12}$$

where H_i is the correlated value of maximum Von Mises stress σ_{vm} found in the structure, and thickness at point i, while thickness of run j is described at as $t_{i,j}$ with bar $\bar{}$ describing the mean value of each term.

2.2.2 Applying the correlation pattern to fatigue behavior

Patterns obtained in Sect. 2.2.1 can not be used directly; it gives a correlation pattern with values in the range [− 1, 1]. This pattern is normalized to the range [0,1]. Such a normalized pattern can easily be used to vary the thickness in the structure into a specified range as

$$t_i = t_{min} + \left(t_{max} - t_{min}\right)\hat{H}_i, \tag{13}$$

where $\hat{H}_i$ is the value of the normalized correlation pattern at point i. Directly applying Eq.(13) to the structure will most likely change the volume of the structure. Retaining the original volume, and therefore mass requires a scaling parameter m, extending Eq.(13) to

$$t_i = t_{min} + (t_{max} - t_{min})\hat{H}_i^m. \tag{14}$$

For each range $t \in \left[t_{min}, t_{max}\right]$ there exists a unique value of m where the volume of the original structure is retained. This value can be obtained numerically using numerical optimization and scalar minimization algorithms, within this paper; Brent's method [2] is used.

3 Numerical analysis

To demonstrate the approach of Sect. 2, a numerical example was analyzed. The structure analyzed is an open-hole specimen, its baseline design is shown in Fig. 1. While this structure does not include bending stresses it does represent an easily reproducible stress state which can be repeated fairly easily. Nothing in the approach suggests that it does not work on more complex structures which include bending stresses. This structure is first modeled in finite elements, after which the approach described in Sect. 2 is used to improve the number of cycles until initial fatigue failure by redistributing the thickness of the structure. An additional study is done to analyze changes in stochastic response. Both the baseline

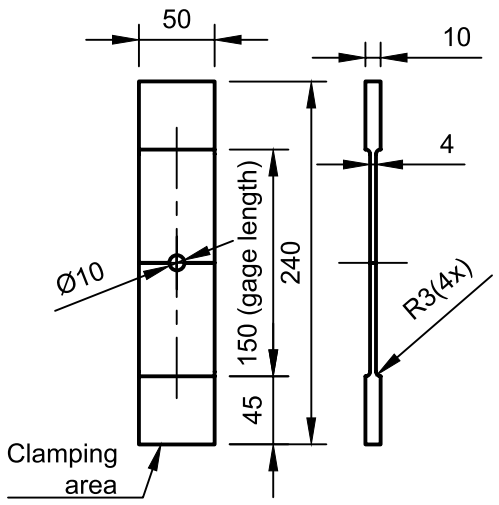

Fig. 1 Drawing of baseline specimen, dimensions in mm

and the improved design were then tested experimentally to demonstrate the potential use of this approach.

3.1 Finite element model

Modeling of the structure in finite elements is done using DIANA FEA [10]. A mean mesh sizing of 1 mm was used to generate a mesh of a quarter of the sample's gage length using 1858 Q8MEM linear shell elements. An image of the discretization can be found in Fig. 2.

The Young's modulus in printed structures depends on both printer settings and build direction [1, 5, 26, 33]. The assumptions listed in section 2.2 means that the qualitative response or improvement should not be affected by anisotropy, assuming the primary build direction and print parameters are maintained in the designs. Therefore, properties used in the analyses shown are assumed based on averaged experimental data in literature as $E = 3.368$ GPa and $\nu = 0.366$. It is important to note that the actual Young's modulus used in the numerical analysis does not significantly affect the linear analyses used to find the correlation between the highest stresses and local changes. Using the unifying fatigue curve for Polylactic Acid (PLA) proposed by [13] a relationship can be made between the maximum stress $\sigma_{max} = \sigma_{mean} + \sigma_{amp}$ relative to the ultimate tensile stress, and the approximate number of cycles until failure. Stresses in the specimen are expected to be minimal in the printing direction, while the ultimate stress in the printing plane is very similar. Figure 3 shows the expected number of cycles for stresses in the printing plane.

Symmetry boundary conditions are applied to the structure on its symmetry line. The left edge in Fig. 2 is fixed in the x-direction, the upper edge is fixed in the y-direction. The rigid body mode in the z-direction is fixed on the edge of the hole. The load is applied as a distributed tensile force on the bottom edge of 1 kN. Von Mises stress results and

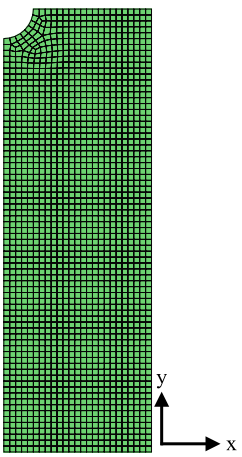

Fig. 2 Mesh discretization

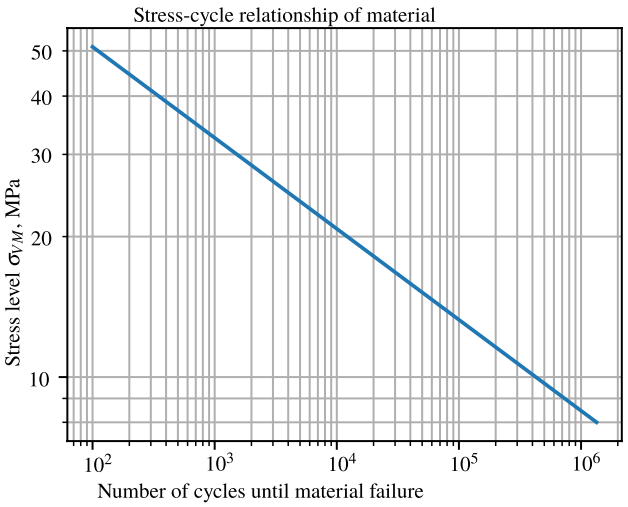

Fig. 3 SN curve used to approximate the number of cycles until initial failure in printing plane of printed PLA

the corresponding number of cycles estimated from the SN-curves of [13] for the baseline sample is shown in Fig. 4.

3.2 Increasing cycles until initial failure

Improvement of the baseline design is achieved using the approach described in Sect. 2.2. Thickness variations are applied through both the type I and type II correlation functions defined in Eqs.(2) and (3) with a correlation length of 5 mm. Figure 5 shows the relationship of distance to the correlation of field values. The correlation length helps

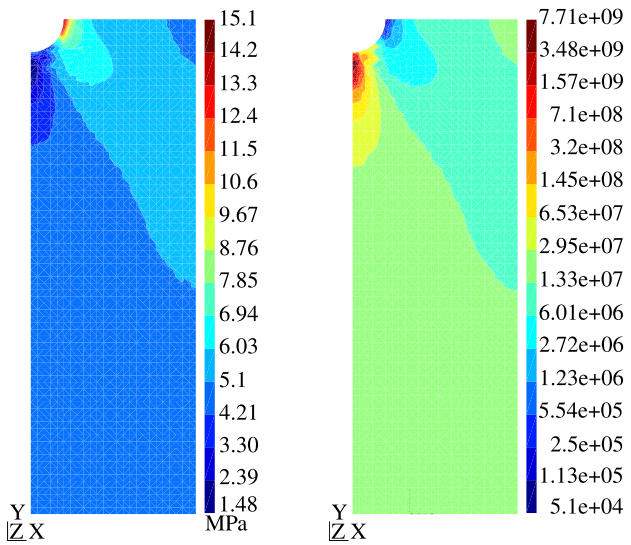

(a) Von Mises stress σ_{VM} (b) Number of cycles until initial failure (logarithmic)

Fig. 4 Baseline results of the finite element model

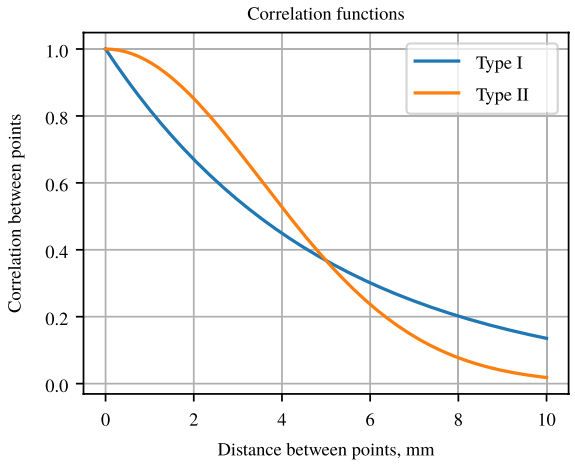

Fig. 5 Correlation functions used to generate thickness patterns, Eqs. (2) and (3) with $L_c = 5$ mm

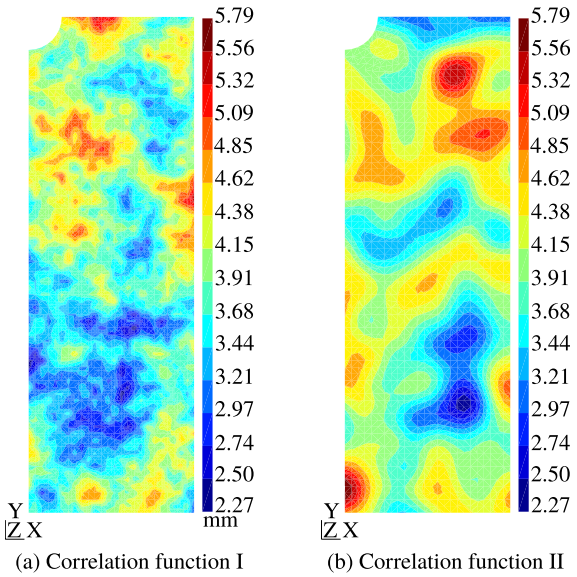

(a) Correlation function I (b) Correlation function II

Fig. 6 Example of thickness distributions generated with two different correlation functions

determine how much distance is needed for the correlation pattern to change significantly within this approach. 5 mm gives reasonably local changes without any very abrupt changes. Fields define the thickness with a standard deviation of $t_\sigma = 0.5$ mm from the $t_\mu = 4$ mm baseline configuration. Changes applied are purely fictitious and only used to generate a correlation pattern. These values can be smaller or slightly larger as long as the response to the local change remains linear. Both of these correlation functions are used to generate two sets with 5000 samples each. The number of samples used was determined by optically checking when the correlation pattern converged and then rounding up. Figure 6 shows an example of a sample of each set.

To find the relative effect of thickness to initial fatigue failure, the Von Mises stress, and the corresponding number of cycles from Fig. 3 are calculated at every node. As described in Fig. 2.2 the initial failure is assumed to be defined by the maximum Von Mises stress and has a logarithmic direct relationship to the number of load cycles. Figure 7 shows the patterns of both types I and II correlation functions and the autocorrelation of each point.

The stress and cycles until failure patterns create a very similar pattern for each correlation function; this is expected as the number of cycles is defined as a function of the stress level. The number of cycles until failure increases with an increase of thickness while the stress decreases. Due to this, the correlation patterns are inverses of each other. Correlation patterns generated using a type II correlation function result in an overall smoother pattern; this is due to the higher correlation the function has at shorter distances (Fig. 5).

Both correlation patterns are used to generate a thickness distribution varying within the range of 2–6 mm. In order to retain the original volume of the structure, the scaling parameter m defined in Eq.(14) had to be computed. Computed values were $m_I = 0.397$ for the type I field and $m_{II} = 0.411$ for the type II field. Figure 8 shows the thickness distributions obtained as well as the new stresses and cycles until initial failure related to the stresses in the structure.

Both patterns are similar and reinforce the hole in the high-stress area by increasing the thickness locally and reducing material in the low-stress area. The solution found can be deduced quite quickly to be more efficient than one obtained by simply adding thickness concentrically around the hole. Stresses vary in the topography around the hole, and sensitivity to local changes also varies significantly over the surface of the structure. Stresses at the top and bottom of the hole are very low, for instance, as forces flow around the hole as shown in Fig. 4a.

Comparing thickness patterns obtained through both correlation functions shows that they are slightly different. Type I correlation function results in a pattern which is less smooth overall, due to the lower correlation to nearby points. Table 1 gives an overview of how the results compare to each other. Both of the improved designs show a decreased stress of 36–38%, which results in having over 10× the number of cycles until initial fatigue failure in Fig. 3.

3.3 Robustness analysis

Designs of Sect. 3.2 are found using random variations, but no analyses are done on the stochastic response of the structure. Robust design can be defined as removing the negative effects of random variations on the performance of a structure. For the current design, this can be interpreted as the distribution of fatigue life in the presence of random thickness variations.

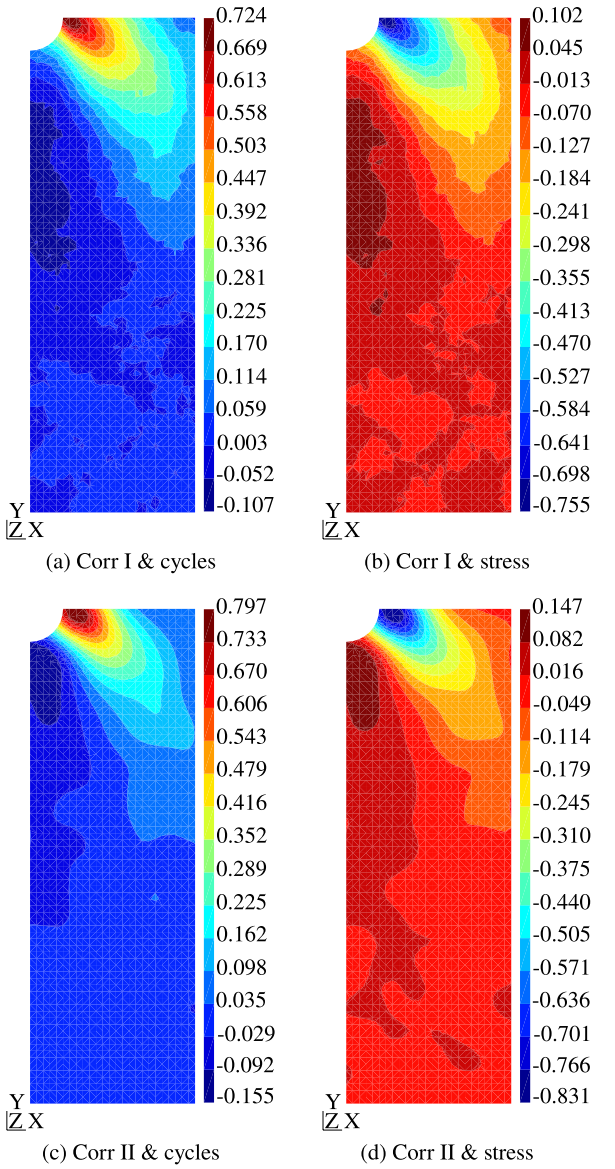

Fig. 7 Correlation patterns of type I and II correlation functions and the stress and number of cycles until initial failure

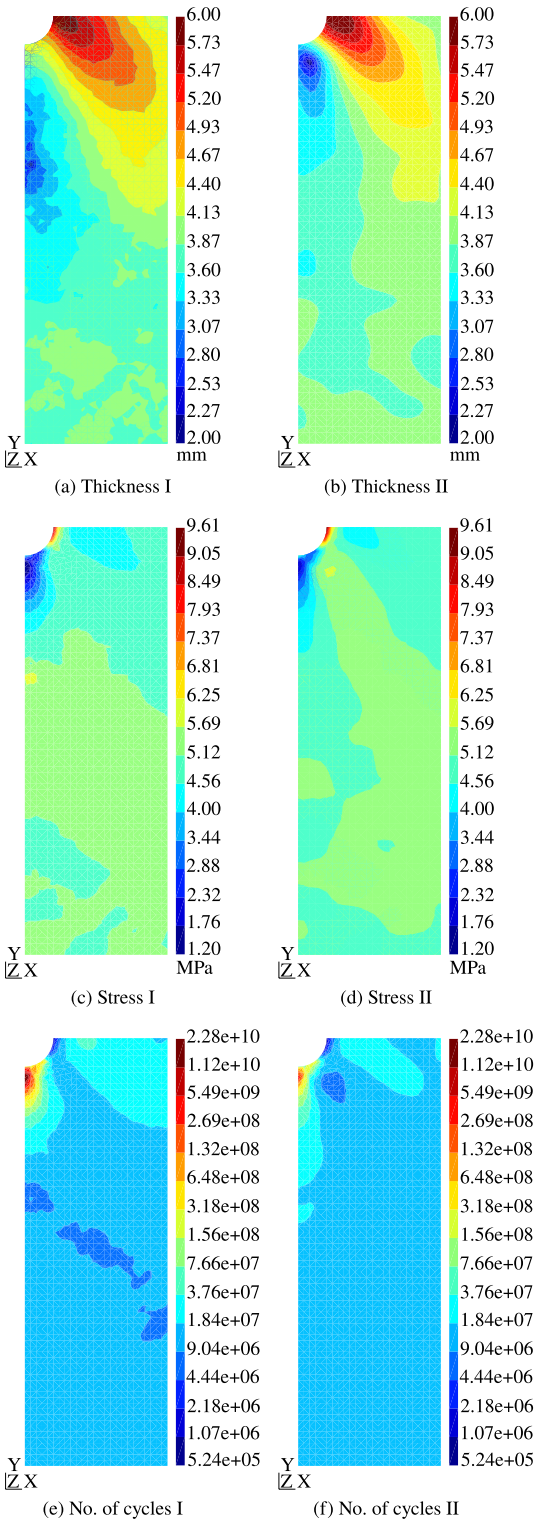

Fig. 8 Thickness distribution, Von Mises stress results and corresponding number of cycles until initial fatigue failure for designs obtained with type I and II correlation functions

Robustness is analyzed by applying thickness variations generated using the same parameters as the thickness variations of Sect. 3.2, with two different correlation functions $t_\sigma = 0.5$ mm and $L_c = 5$ mm. These variations are applied to the baseline design, as well as the enhanced designs. The results of the maximum stress analyses are shown in Table 2. The statistical properties are shown for a normal distribution with a coefficient of variation (CoV) defined as $\text{CoV} = \frac{\sigma}{\mu}$. Estimated cycles until failure has been fit to a lognormal distribution, the parameters of the natural logarithm of these distributions are shown in Table 3,

Table 1 Comparison between the maximum Von Mises stress and corresponding number of cycles until initial failure for baseline and enhanced designs

	σ_{VM}		Cycles	
Baseline	15.1 MPa	–	5.1E4	–
Pattern I	9.35 MPa	− 38.1%	6.02E5	11.8×
Pattern II	9.61 MPa	− 36.4%	5.24E5	10.3×

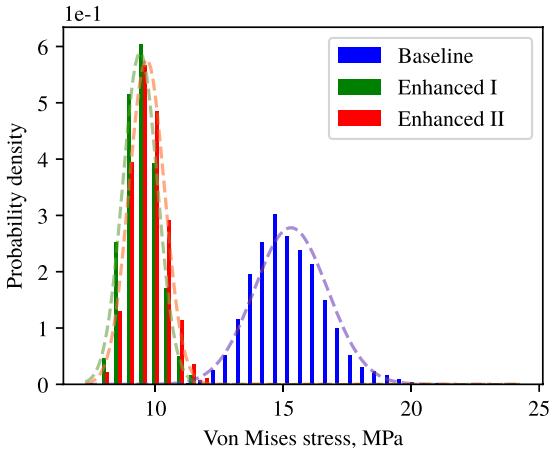

Fig. 9 Probability density function of maximum stress in structure subjected to type I thickness variations

Fig. 10 Probability density function of expected number of cycles until initial failure for structure subjected to type I thickness variations

where the coefficient of variation for lognormal distributions is defined as $\text{CoV} = \sqrt{e^{\sigma^2} - 1}$.

Enhancing the design has caused not only the deterministic design to be improved, but also has reduced the standard deviation of the response, significantly improving structural reliability. Figure 9 shows the normal distributions found, as well as a histogram of the 5000 analyses of baseline and enhanced designs. Distributions of the enhanced and baseline designs only have a small overlap at the tail of the distribution. Reducing the maximum stress in the structure greatly influences the expected number of cycles until initial failure. The lognormal distribution of cycles is shown in Fig. 10, showing that the expected number of cycles is approximately one order of magnitude higher for the enhanced designs.

4 Experimental validation

The numerical results of Sect. 3 show a great increase in the expected fatigue life of specimens with the specified thickness redistribution. Manufacturing panel structures with tailored thicknesses using a traditional manufacturing process is quite challenging, requiring multiple machining steps. This section tries to analyze the potential use of additive manufacturing to generate structures with these types of thickness redistributions.

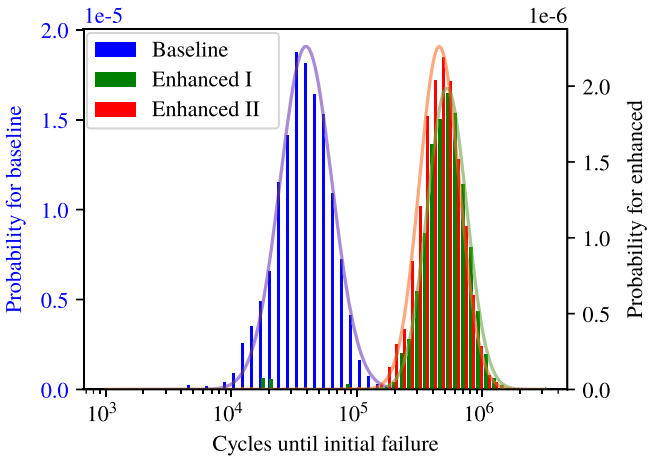

Table 2 Statistical stress σ_{VM} properties baseline and enhanced designs subjected to thickness variations generated with type I and II correlation functions with $L_c = 5$ mm and $t_\sigma = 0.5$ mm

	Thickness variations of type I						Thickness variations of type II					
$X = \mu + \sigma Z$	μ, MPa	δ	σ, kPa	δ	CoV	δ	μ, MPa	δ	σ, kPa	δ	CoV	δ
Baseline	15.30	(–)	1430	(–)	9.35%	(–)	15.31	(–)	1470	(–)	9.60%	(–)
Enhanced I	9.40	(− 38.6%)	678	(− 52.6%)	7.22%	(− 22.8%)	9.39	(− 38.7%)	683	(− 53.5%)	7.27%	(− 24.3%)
Enhanced II	9.66	(− 36.9%)	692	(− 51.6%)	7.17%	(− 23.3%)	9.65	(− 37.0%)	700	(− 52.4%)	7.26%	(− 24.4%)

Table 3 Statistical parameters of the number of cycles until failure distribution's natural logarithm, of baseline and enhanced designs subjected to thickness variations generated using type I and II correlation functions with $L_c = 5$ mm and $t_\sigma = 0.5$ mm

	Thickness variations of type I						Thickness variations of type II					
$X = e^{\mu+\sigma Z}$	μ	δ	σ	δ	CoV	δ	μ	δ	σ	δ	CoV	δ
Baseline	10.81	(–)	0.475	(–)	0.503	(–)	10.80	(–)	0.485	(–)	0.515	(–)
Enhanced I	13.29	(− 22.9%)	0.361	(− 24.0%)	0.361	(− 25.8%)	13.30	(− 23.1%)	0.365	(− 24.7%)	0.378	(− 26.6%)
Enhanced II	13.16	(− 21.7%)	0.365	(− 23.2%)	0.378	(− 24.9%)	13.16	(− 21.9%)	0.370	(− 23.7%)	0.383	(− 25.6%)

The test campaign contained two types of tests. The first test has the objective of finding the failure load. Researchers have already published the ultimate tensile stress of PLA structures produced with FFF, but the numbers vary from 15.5–72.2 MPa [21, 24], depending on the chosen filament and production parameters [5, 37]. As the objective of the test is to observe an increase in fatigue life of the structure, it is not necessary to obtain an exact tensile strength for the experimental campaign. What does have to be obtained is an appropriate load level to perform the fatigue test on, this is done by performing a static test series.

Using a load level derived from the static test, an oscillating sinusoidal load with varying amplitude ($R = \frac{F_{min}}{F_{max}} = 0.1$) is applied to the structure until structural failure occurs. This fatigue test is first done on the baseline constant thickness sample and then repeated with the redesigned sample featuring a thickness redistribution.

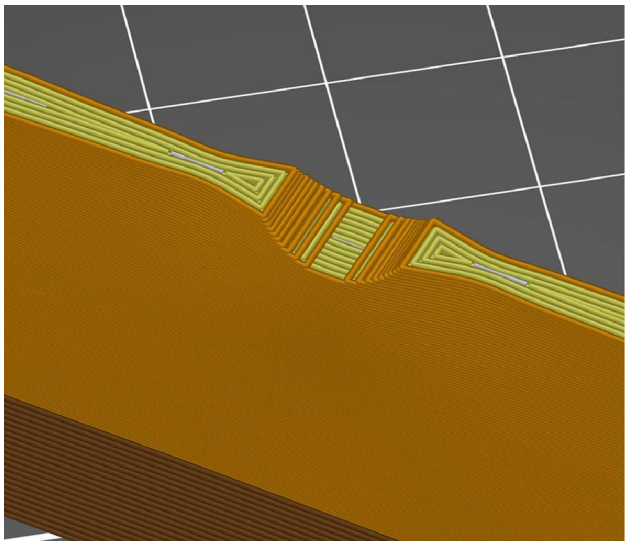

Fig. 11 Orientation of filament in the printing of the improved sample

4.1 Test specimen manufacturing using FFF technique

Samples were manufactured by importing the design from Sect. 3 and adding transitional radii between the clamping and gage areas. Sample manufacturing was done using the FFF technique and Polylactic Acid (PLA) filament.

Manufacturing of the samples was done at the institute of adaptronics and function integration (IAF) of TU Braunschweig. Using a nozzle diameter of 0.4 mm, a heating chamber temperature of 220 °C, and a print bed temperature of 55 °C. The layer height used during printing was 0.2 mm.

The test specimens were printed as solid pieces, while most filament strands in the gauge area are routed in the direction of force with the help of a concentric arrangement as shown in Fig. 11. The test samples were spray-painted with a speckled pattern after printing, for deformation tracking with a digital image correlation system, as is visible in Fig. 12.

4.2 Test setup

Tests were performed at the testing facility of the Institute of Structural Analysis in Hannover, Germany. Samples were tested in a servo-hydraulic test machine with an attached 12.5 kN load cell. The machine clamps the sample on both ends, as shown in Fig. 12, where the bottom end is free in rotation, eliminating any unwanted torque in the test setup.

A digital image correlation (DIC) system constantly monitored the sample during testing. This system allows for real-time tracking of displacements (and resulting strains) of the test sample. Within the fatigue tests, the hole elongation is measured as a measure of damage evolution. An overview of the system operating during testing is shown in Fig. 13.

4.3 Static pretesting

The goal of the static test series is to find an appropriate load level for the succeeding fatigue test series. During the test, specimens were elongated at a rate of 1 mm/min, while continually recording the resulting force. The test was repeated 3 times, and showed a high degree of reproducibility, with ultimate loads of around 8.5 kN. The force-displacement graphs of these three tests can be found in Fig. 14.

Fig. 12 Test sample clamped into test machine

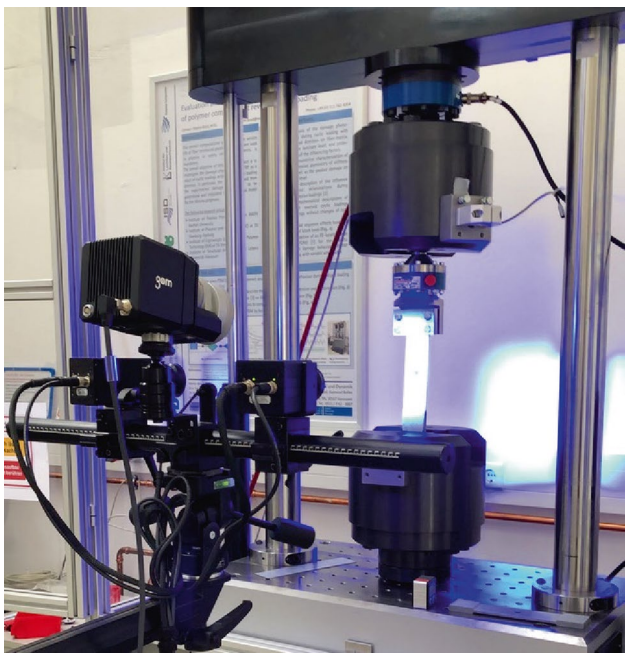

Fig. 13 Test setup with digital image correlation system

Pretesting determines an appropriate load level and indicates reproducibility. As tests on the improved samples are performed on the same load levels, pretesting is not repeated for those designs.

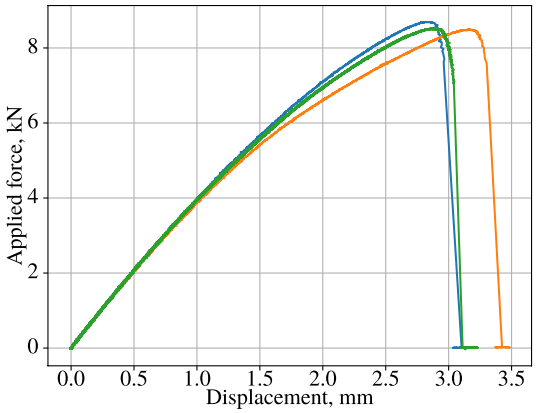

Fig. 14 Static pretest results of baseline samples

4.4 Fatigue testing

In order to assess the fatigue performance of both designs fatigue tests are performed under an oscillating load until failure. Force is applied as a sinusoid with a load level of 25%, 50% and 70% of the ultimate load of Fig. 4.3, and a minimum load of a tenth of that, giving a stress ratio of $R = \frac{F_{min}}{F_{max}} = 0.1$.

At least three samples are used at each load level. The data points were used to fit a curve using the Basquin equation of $N = \frac{B}{S_r^m}$, where N is the number of cycles, S the stress level, B and m are fitting parameters. A curve was fit using the Levenberg-Marquardt algorithm, leading to the following least-squares fits

$$N_{BL} = \frac{340.58}{S_r^{4.49}}, \tag{15}$$

for the baseline sample and

$$N_{Imp} = \frac{1661.9}{S_r^{4.24}}, \tag{16}$$

for the improved sample.

The results shown in Fig. 15 make it clear that the redistributed thickness found in Sect. 3 results in a significant improvement in the fatigue life. Accurately quantifying this improvement requires more testing, but it seems to be in the order of 4 to 5 times the original design on average.

The spread between results is relatively small. Tests done by [11] show an order of magnitude difference between the top and bottom 10% of samples. Results of the experiments performed in this paper all show a difference of the highest and lowest results of less than an order of magnitude. Any possible effects the load level has on this spread can not be extrapolated from the data as the sample size is not large enough.

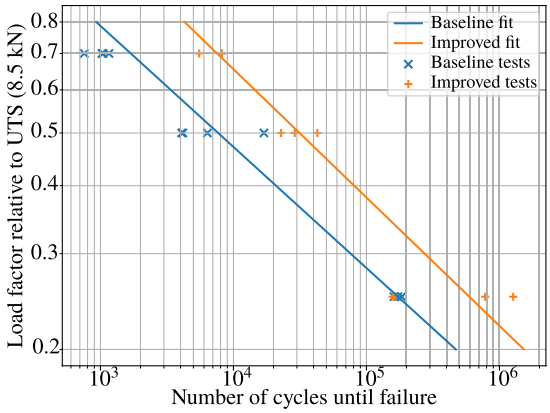

Fig. 15 SN data of tested specimens and fitted curves

4.4.1 Analysis of fatigue failure of specimens

Failure in the numerical studies was taken as an instantaneous event, without any progressive damage, which can cause stresses to redistribute. Within this section, this assumption is analyzed using data obtained during testing. Hole elongation is used as a measure of damage progression. The relative progression towards failure is shown in Fig. 16. Within this diagram, the elongation of the hole is plotted using a virtual extensometer generated using digital image correlation during testing. Values in the y-direction are set to

$$D = \frac{\frac{F_1}{u_1}}{\frac{F_n}{u_n}} = \frac{F_1 u_n}{F_n u_1} \triangleq \frac{E_1}{E_n}, \tag{17}$$

where values $\frac{F_1}{u_1}$ is the original stiffness, and $\frac{F_n}{u_n}$ the apparent stiffness during the test. The original stiffness is calculated as the average stiffness as the load is increased from 1 to 25% of the maximum load level at the start of the test.

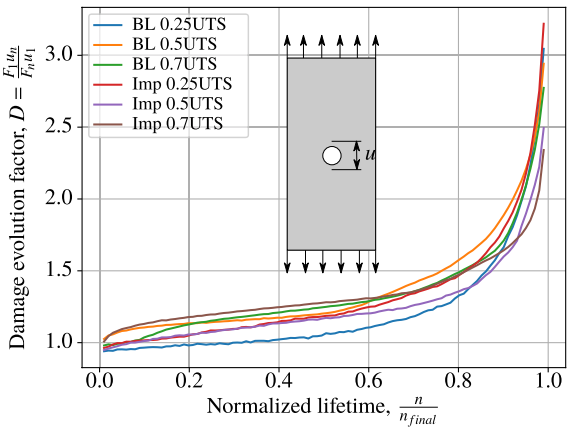

Fig. 16 Evolution of apparent elasticity during testing

Figure 16 shows that there is a significant amount of progressive damage, and therefore stress redistribution during testing. Stress redistribution and internal damage cause the stress distribution to evolve during the lifetime of the structure. The figures show an approximately linear increase in the damage evolution up to 60-80% of their lifetime. At this point, stress redistribution and crack forming cause an accelerated increase in the damage evolution until final failure occurs. Numerical analysis of Sect. 3 does not take any evolution or stress redistribution into account.

The mechanism resulting in ultimate failure seems to be identical in the baseline and improved designs. Relative progression of damage shown in Fig. 16 shows that the evolutionary characteristic of damage is very similar. Samples also showed cracks initiate at the same areas within both designs. It is, therefore, reasonable to assume that the primary mechanism leading to fatigue life improvement is the reduced tensile stress at critical locations. Lowering the stresses results in a slowing down damage progression and increase in the structural lifespan.

Also, fracture initiation found in the samples is not in the highest stress area in the finite element model. Figure 4 shows that the highest von Mises stress in the structure is at the 3 and 9 o'clock locations of the hole. Fractures in the tested specimens were shown to initiate slightly above or below this location, i.e., 2, 4, 8, or 10 o'clock positions. Figure 17 shows a typical fracture forming during testing. The topography of the immediate area can be seen in Fig. 11. The area that was found most critical in the finite element analysis consists of filaments oriented in the tensile direction. Immediately to the side of the critical areas, transversely oriented filaments effectively introduce notches into the structure. Notches such as these naturally attract stress concentrations, leading to crack initiation and crack growth leading to final failure. Such topological features are not included within the numerical model. The structure is modeled using ideal geometry. Manufacturing with FFF means

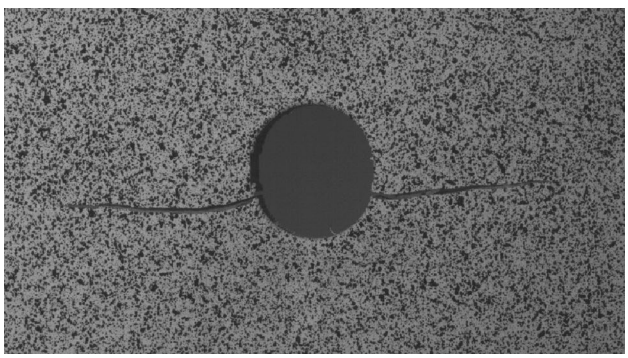

Fig. 17 Evolving crack pattern formed during testing, just before final failure

that the actual topology differs, making it easy for stresses to concentrate at irregularities not included in the model.

5 Conclusion and discussion

This paper has presented a numerical approach to increase the fatigue life of structures by tailoring the distribution of local thickness. By applying this approach to a test specimen, the simulated fatigue life was increased by order of magnitude. Numerical results also show that the approach decreases the sensitivity of the structure to random variations of thickness.

Experiments showed the potential use of this approach on structures manufactured using additive techniques. The experiments show that the number of cycles until failure is increased to around 4 to 5 the original baseline design. The method discussed is not designed to predict the number of cycles until failure but only to improve it. Nevertheless, analyzing this difference can show how the approach can be extended to include other effects.

This discrepancy between numerical and experimental results could be resolved by extending the fatigue model to consider additional effects. The two main areas identified are printer orientation and stress redistribution. Extending the numerical model to take these effects into account will likely improve the experimental results.

Additive manufacturing using FFF causes a topology within the final structure that can have areas more sensitive to crack initiation. The printing layup can be adapted to remove these sensitive areas if this is considered in the numerical model. In cases where the topology must have these sensitive areas, the stresses can be lowered by adopting a scaling function to the fatigue relation used to generate a correlation pattern.

Compared to standard topology optimization methods used in additive manufacturing [14, 29], the approach discussed in this paper differentiates itself by including stochastic variations in the design. By including these, the design can become more robust towards imperfections and enable evaluation of robustness during and after design using the same procedure. In addition to this, a transitory length scale can be specified through a correlation function and length used to generate variations. These length scales can assure continuity of thickness patterns, making it easier to assure manufacturability. Solutions obtained using density-based topology optimization may also create additional holes or end up with lattice-type solutions instead of continuous surfaces, which may be undesirable in structures such as wings panels. Extensive quantitative comparisons between approaches are left for the next phase of development.

Though this paper only deals with improving the fatigue life by redistributing the material thickness, it is possible to have a similar approach towards other parameters in AM. Process parameters, such as print speed, can directly affect the quality of a printed structure. The optimal values are usually a compromise between manufacturing time and quality. A similar analysis to that done in this paper could be performed to tailor the local use of process parameters, increasing the manufacturing speed while retaining high accuracy and a good finish in critical areas.

Acknowledgments The authors thank Gerd-Jan Schreppers from DIANA FEA B.V. for his support with the numericalanalyses in DIANA. Our final thanks go to Christian Gerendt, Martin Brod, Oliver Dorn, and JensBreyer for their assistance in experimental work.

Funding Open Access funding enabled and organized by Projekt DEAL. We would like to acknowledge the funding by the Deutsche Forschungsgemeinschaft (DFG, German Research Foundation) under Germany's Excellence Strategy-EXC 2163/1- Sustainable and Energy Efficient Aviation-Project-ID 390881007.

Data availability Test data and numerical results are available upon request

Code availability Results are generated using DIANA, a commercially available finite element solver, pre and postprocessing is done using a series of python scripts. These python scripts can be made available to researchers upon request.

Declarations

Conflict of interest The authors declare that they have no conflict of interest.

References

1. Afrose MF, Masood SH, Iovenitti P, Nikzad M, Sbarski I (2016) Effects of part build orientations on fatigue behaviour of FDM-processed PLA material. Prog Addit Manuf 1(1–2):21–28. https://doi.org/10.1007/s40964-015-0002-3
2. Brent RP (2013) Algorithms for minimization without derivatives. Courier Corporation
3. van den Broek S, Minera S, Pirrera A, Weaver PM, Jansen E, Rolfes R (2020) Enhanced deterministic performance of panels using stochastic variations of geometry and material. AIAA J 58(5):2307–2320. https://doi.org/10.2514/1.J058962

4. van den Broek S, Minera S, Jansen E, Rolfes R (2021) Robust improvement of the asymmetric post-buckling behavior of a composite panel by perturbing fiber paths. Compos Struct 270:114011. https://doi.org/10.1016/j.compstruct.2021.114011
5. Chacón JM, Caminero MA, García-Plaza E, Núñez PJ (2017) Additive manufacturing of PLA structures using fused deposition modelling: effect of process parameters on mechanical properties and their optimal selection. Mater Des 124:143–157. https://doi.org/10.1016/j.matdes.2017.03.065
6. Chacón JM, Caminero MA, Núñez PJ, García-Plaza E, García-Moreno I, Reverte JM (2019) Additive manufacturing of continuous fibre reinforced thermoplastic composites using fused deposition modelling: effect of process parameters on mechanical properties. Compos Sci Technol 181:107688. https://doi.org/10.1016/j.compscitech.2019.107688
7. Dapogny C, Estevez R, Faure A, Michailidis G (2019) Shape and topology optimization considering anisotropic features induced by additive manufacturing processes. Comput Methods Appl Mech Eng 344:626–665. https://doi.org/10.1016/j.cma.2018.09.036
8. Davis MW (1987) Production of conditional simulations via the LU triangular decomposition of the covariance matrix. Math Geol 19(2):91–98. https://doi.org/10.1007/BF00898189
9. Dekking FM, Kraaikamp C, Lopuhaä HP, Meester LE (2005) A modern introduction to probability and statistics: understanding why and how. Springer Science & Business Media. https://doi.org/10.1007/1-84628-168-7
10. Diana FEA (2020) DIANA Finite Element Analysis User's Manual Release 10.4. Tech. rep., Delft, the Netherlands. https://dianafea.com/manuals/d104/Diana.html. Accessed 1 July 2021
11. Ezeh OH, Susmel L (2018) Fatigue behaviour of additively manufactured polylactide (PLA). Procedia Struct Integr 13:728–734. https://doi.org/10.1016/j.prostr.2018.12.121
12. Ezeh OH, Susmel L (2018) On the fatigue strength of 3D-printed polylactide (PLA). Procedia Struct Integr 9:29–36. https://doi.org/10.1016/j.prostr.2018.06.007
13. Ezeh OH, Susmel L (2019) Fatigue strength of additively manufactured polylactide (PLA): effect of raster angle and non-zero mean stresses. Int J Fatigue 126:319–326. https://doi.org/10.1016/j.ijfatigue.2019.05.014
14. Fu YF (2020) Recent advances and future trends in exploring Pareto-optimal topologies and additive manufacturing oriented topology optimization. Math Biosci Eng 17(5) 4631–4656. https://doi.org/10.3934/mbe.2020255
15. Gao W, Zhang Y, Ramanujan D, Ramani K, Chen Y, Williams CB, Wang CC, Shin YC, Zhang S, Zavattieri PD (2015) The status, challenges, and future of additive manufacturing in engineering. CAD Comput Aided Des 69:65–89. https://doi.org/10.1016/j.cad.2015.04.001
16. Gibson I, Rosen DW, Stucker B (2010) Additive manufacturing technologies. Springer Science & Business Media. https://doi.org/10.1007/978-1-4419-1120-9
17. Van der Have R (2015) Random fields for non-linear finite element analysis of reinforced concrete. http://repository.tudelft.nl/islandora/object/uuid:25780e9a-49c4-4085-9a65-af73119d97a7?collection=education. Accessed 1 July 2021
18. Hristopulos D (2020) Random fields for spatial data modeling. Springer Nature B.V. https://doi.org/10.1007/978-94-024-1918-4
19. Iragi M, Pascual-González C, Esnaola A, Lopes CS, Aretxabaleta L (2019) Ply and interlaminar behaviours of 3D printed continuous carbon fibre-reinforced thermoplastic laminates; effects of processing conditions and microstructure. Addit Manuf. https://doi.org/10.1016/j.addma.2019.100884
20. Keshavarzzadeh V, Kirby RM, Narayan A (2020) Stress-based topology optimization under uncertainty via simulation-based Gaussian process. Comput Methods Appl Mech Eng 365:112992. https://doi.org/10.1016/j.cma.2020.112992
21. Kotlinski J (2014) Mechanical properties of commercial rapid prototyping materials. Rapid Prototyp J 20(6):499–510. https://doi.org/10.1108/RPJ-06-2012-0052
22. Kriegesmann B, Rolfes R, Hühne C, Teßmer J, Arbocz J (2010) Probabilistic design of axially compressed composite cylinders with geometric and loading imperfections. Int J Struct Stab Dyn 10(04):623–644. https://doi.org/10.1142/S0219455410003658
23. Langelaar M (2016) Topology optimization of 3D self-supporting structures for additive manufacturing. Addit Manuf 12:60–70. https://doi.org/10.1016/j.addma.2016.06.010
24. Lanzotti A, Grasso M, Staiano G, Martorelli M (2015) The impact of process parameters on mechanical properties of parts fabricated in PLA with an open-source 3-D printer. Rapid Prototyp J 21(5):604–617. https://doi.org/10.1108/RPJ-09-2014-0135
25. Lazarov BS, Wang F (2017) Maximum length scale in density based topology optimization. Comput Methods Appl Mech Eng 318:826–844. https://doi.org/10.1016/j.cma.2017.02.018
26. Letcher T (2014) Material Property Testing of 3D-printed Specimen in PLA on an Entry-level 3D Printer. In: Proceedings of the ASME 2014 International Mechanical Engineering Congress & Exposition IMECE2014, pp 1–8
27. Liu S, Li Q, Chen W, Tong L, Cheng G (2015) An identification method for enclosed voids restriction in manufacturability design for additive manufacturing structures. Front Mech Eng 10(2):126–137. https://doi.org/10.1007/s11465-015-0340-3
28. Lyons B (2014) Additive manufacturing in aerospace: examples and research outlook. Bridge 42(1):13–19. https://www.nae.edu/58467/Additive-Manufacturing-in-Aerospace-Examples-and-Research-Outlook. Accessed 11 April 2022
29. Meng L, Zhang W, Quan D, Shi G, Tang L, Hou Y, Breitkopf P, Zhu J, Gao T (2020) From topology optimization design to additive manufacturing: today's success and tomorrow's roadmap. Arch Comput Methods Eng 27(3):805–830. https://doi.org/10.1007/s11831-019-09331-1
30. Picelli R, Townsend S, Brampton C, Norato J, Kim HA (2018) Stress-based shape and topology optimization with the level set method. Comput Methods Appl Mech Eng 329:1–23. https://doi.org/10.1016/j.cma.2017.09.001
31. Qian X (2017) Undercut and overhang angle control in topology optimization: a density gradient based integral approach. Int J Numer Methods Eng 111(3):247–272. https://doi.org/10.1002/nme.5461
32. Shinozuka M, Deodatis G (1996) Simulation of multi-dimensional Gaussian stochastic fields by spectral representation. Appl Mech Rev 49(1):29–53. https://doi.org/10.1115/1.3101883
33. Song Y, Li Y, Song W, Yee K, Lee KY, Tagarielli VL (2017) Measurements of the mechanical response of unidirectional 3D-printed PLA. Mater Des 123:154–164. https://doi.org/10.1016/j.matdes.2017.03.051
34. Spanos PD, Zeldin BA (1998) Monte carlo treatment of random fields: a broad perspective. Appl Mech Rev 51(3):219. https://doi.org/10.1115/1.3098999
35. Sudret B, Der Kiureghian A (2000) Stochastic Finite Element Methods and Reliability: A State-of-the-Art Report. University of California Berkeley (November):189, https://ethz.ch/content/dam/ethz/special-interest/baug/ibk/risk-safety-and-uncertainty-dam/publications/reports/SFE-report-Sudret.pdf. Accessed 11 Apr 2022
36. Vanmarcke E, Grigoriu M (1983) Stochastic finite element analysis of simple beams. J Eng Mech 109(5):1203–1214. https://doi.org/10.1061/(asce)0733-9399(1983)109:5(1203)
37. Wittbrodt B, Pearce JM (2015) The effects of PLA color on material properties of 3-D printed components. Addit Manuf 8:110–116. https://doi.org/10.1016/j.addma.2015.09.006
38. Wu W, Geng P, Li G, Zhao D, Zhang H, Zhao J (2015) Influence of layer thickness and raster angle on the mechanical properties of

3D-printed PEEK and a comparative mechanical study between PEEK and ABS. Materials 8(9):5834–5846. https://doi.org/10.3390/ma8095271

39. Zhou M, Lazarov BS, Wang F, Sigmund O (2015) Minimum length scale in topology optimization by geometric constraints. Comput Methods Appl Mech Eng 293:266–282. https://doi.org/10.1016/j.cma.2015.05.003
40. Zou R, Xia Y, Liu S, Hu P, Hou W, Hu Q, Shan C (2016) Isotropic and anisotropic elasticity and yielding of 3D printed material. Compos B Eng 99:506–513. https://doi.org/10.1016/j.compositesb.2016.06.009